LETTER • OPEN ACCESS

Scattering-free Ce:LYBO single crystals for thermal neutron detection

OPEN ACCESS

Applied Physics Express 17, 015502 (2024) LETTER

https://doi.org/10.35848/1882-0786/ad1892

Scattering-free Ce:LYBO single crystals for thermal neutron detection

Dongsheng Yuan[1*], Encarnación G. Víllora[1], Daisuke Nakauchi[2], Takumi Kato[2], Noriaki Kawaguchi[2], Takayuki Yanagida[2], and Kiyoshi Shimamura[1]

[1]National Institute for Materials Science, 1-1 Namiki, Tsukuba, Ibaraki 305-0044, Japan
[2]Nara Institute of Science and Technology, 8916-5 Takayama-cho, Ikoma, Nara 630-0192, Japan

*E-mail: yuan.dongsheng@nims.go.jp

Received December 18, 2023; revised December 21, 2023; accepted December 24, 2023; published online January 17, 2024

$Ce:Li_6Y(BO_3)_3$ (LYBO) is a well-known candidate for thermal neutron detection with a very high Li concentration ($3.06 \times 10^{22}/cm^3$). So far, as-grown crystals exhibit a milky appearance that compromises their performance as scintillators. Current work demonstrates, for the first time, the growth of scattering-free undoped and Ce-doped LYBO by a thermal quenching process. The origin and features of the scattering centers are investigated in detail. Furthermore, the annealing treatment for the scintillation activation is studied, finding that the reduction in oxygen vacancies is mandatory. Under thermal neutron irradiation, the annealed scattering-free Ce:LYBO single crystal achieves a record-high light yield of 6200 ph/n in a single decay with a lifetime as short as 24 ns. © 2024 The Author(s). Published on behalf of The Japan Society of Applied Physics by IOP Publishing Ltd

Neutron detectors are used for homeland security, oil well-logging, radiation therapy, and fundamental research.[1–4] Among various kinds of detectors, the proportional counters based on gas tanks filled with ^3He or BF_3 are still the most common types. However, besides the desire for more compact and handy detectors, all-solid-state alternatives are in high demand due to the worldwide shortage of ^3He gas, on the one hand, and the corrosive and toxic nature of BF_3 gas, on the other. Among all-solid-state scintillators, Li-based materials have attracted much attention due to their relatively high capture cross-section (σ = 940 barn) and the distinguishable reaction energy ($\sim$ 4.8 MeV) after the interaction between a ^6Li isotope and a neutron. The representative scintillators include Li-glass (with 95% ^6Li enriched GS20 as the most representative one, i.e. a Li content of 1.43×10^{22} cm^{-3}), Li-halides (Eu:LiI, $Ce:Cs_2LiYCl_6$, $Eu:LiCaAlF_6$), and LiF/ZnS composites, etc.[5–9] Though some of them have become commercially available, one or more critical drawbacks still exist, such as a high production cost, serious hygroscopicity, and a long scintillation decay.

Ce-doped $Li_6Y(BO_3)_3$ (LYBO) stands out as a promising alternative.[10,11] Compared with other candidates, it compromises a priori of all required basic material properties: a high Li content (3.06×10^{22} cm^{-3}), good chemical stability, a trivalent site (Y^{3+}) for efficient Ce^{3+} doping, cheap and abundant constituents, and the possibility to grow large single crystals for low-cost mass production. Despite these promising characteristics, the poor crystalline and optical quality of Ce:LYBO crystals has largely discouraged its development for scintillation applications so far.[12–16] Recently, we have demonstrated that a post-growth thermal treatment close to T_m can drastically reduce the milky appearance of crystals while the light yield (LY) rises to 4650 ph/n.[11] Nevertheless, to date it is still unknown, on the one hand, what are the origin and nature of the scattering centers, and on the other hand, what is the annealing mechanism that improves the scintillation response.

In this work, undoped and Ce-doped LYBO crystals were grown as explained previously,[17] and growth and cooling rates were varied to elucidate the origin and nature of scattering centers that lead to the typical milky appearance of LYBO crystals. In the ultimate case, the power generator was switched off after the crystal separation from melt. This new thermal quenching procedure led systematically to scattering-free crystals. This was particularly interesting in Ce-doped crystals since so far Ce-doping had been found to increase the amount of scattering centers. Single crystal plates for characterization were cut along the *b*-plane. Annealing was carried out under air for 15 h at 805 °C while monitoring the sample temperature with a nearby thermocouple. All the samples were fine-polished on both sides before characterization.

The microstructure of LYBO crystals was investigated by high-resolution FE-SEM (JSM-6500F) and AFM (Asylum MFP-3D Origin) on a slightly etched sample. Apart from surface scratches due to polishing, the color contrast observed in FE-SEM images stems from a compositional shift. Regions with a higher effective atomic number Z_{eff} emit and reflect electrons more efficiently and therefore appear in a brighter color. In the following discussion, the Z_{eff} of various compounds is estimated using by the equation:[18]

$$Z_{eff} = \sqrt[4]{\sum w_i * Z_i^4} \quad (1)$$

where w_i is the atomic weight fraction of the *i*th element and Z_i its corresponding atomic number. The density of scattering centers was evaluated visually with a green laser pointer (550 nm, 1 mW), and more in detail with a He-Ne laser (633 nm, 5 mW) and a microscope (OLYMPUS BX51).

Optical transmittance measurements were recorded with Jasco spectrometers. The direct transmission with a V-570 and the total one (direct plus diffused) with a V-770 equipped with an integrating sphere. The elemental analysis was conducted by the inductively coupled plasma optical emission spectroscopy (ICP-OES) Aligent 5800.

X-ray radioluminescence (XRL) spectra and decay were characterized using homemade setups.[19–21] The pulse-height spectra (PHS) were measured under neutron irradiation from ^{252}Cf with a photomultiplier tube (PMT, R7600-U200,

Hamamatsu) operating at 600 V (gain 100, shaping time 0.5 μs). The thermal neutron LY in photons/neutron (ph/n) was calibrated with a commercial ^{6}Li-glass GS20 sample (from Saint-Gobain S.A.), while weighing the results from the multichannel analyzer with the corresponding XRL spectra and the quantum efficiency of the photomultiplier detector.

Scattering centers in as-grown Ce:LYBO crystals can be easily visualized with laser pointers, for example, the light of a green one (550 nm, 1 mW) exhibits a strong scattering path even in slightly milky crystals as shown in our recent work.[11] To investigate the nature of these scattering centers, the microstructure of fine-polished *b*-plane LYBO crystals was investigated by FE-SEM and AFM, as shown in Figs. 1(a) and 1(b), respectively. In both images, elongated structures ~12° tilted from the (−102) cleavage plane are observed, with the long ones having a needle-like appearance of ~1 um in length. These microstructures are observed for the first time, and it is assumed that these are the scattering centers that cause the milky appearance of crystals. As the crystalline nature and composition of these could not be investigated by high-resolution transmission electron microscope and energy-dispersive X-ray spectroscopy, due to the quick sample degradation under the electron beam, at present we cannot confirm the nature of the scattering centers. Nevertheless, from the light-color compositional contrast in FE-SEM and the protuberance in AFM images, it can be deduced that the scattering centers correspond to segregated particles with a higher effective atomic number Z_{eff} and a higher chemical stability than LYBO, respectively. After disregarding Li-borates due to their low Z_{eff}, the following binary and ternary potential oxide compounds that are stable at atmospheric pressure can be considered as potential candidates: $LiYO_2$, YBO_3, YB_3O_6, $LiY_6O_5(BO_3)_3$, $Li_2YB_5O_{10}$, $Li_3Y_2(BO_3)_3$, and $Li_3Y(BO_3)_2$. From Z_{eff} considerations in Table I, $Li_2YB_5O_{10}$ can be excluded due to its lower value than LYBO, while YB_3O_6, $Li_3Y_2(BO_3)_3$, and $Li_3Y(BO_3)_2$ are improbable due to their similar ones. Consequently, only three potential candidates remain: $LiYO_2$, YBO_3, and $LiY_6O_5(BO_3)_3$. The latter is found to segregate at the crucible bottom during the LYBO growth by the Czochralski technique,[17] and at first sight, it was plausible to hypothesize that traces of it present in the melt segregate in the matrix during the growth of LYBO. As will be demonstrated later, this is not the case because scattering centers appear after the LYBO solidification. Furthermore, as the $LiY_6O_5(BO_3)_3$ segregation upon cooling would involve a non-negligible diffusion of Y atoms through the lattice to increase their concentration according to the chemical formula, this compound is tentatively disregarded. Consequently, the simpler $LiYO_2$ and/or YBO_3 remain the most probable compounds to segregate and to be the origin of light scattering. In the later discussion, however, it will be shown that YBO_3 may be disregarded. For now, and before discussing the moment at which the segregation takes place, the concentration of scattering centers in as-grown crystals and annealed ones is considered in the following.

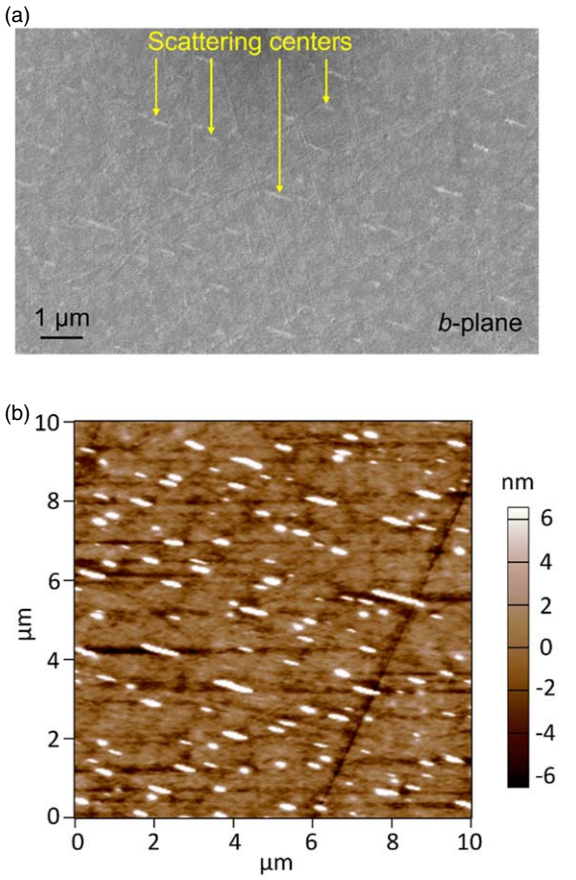

Fig. 1. (a) FE-SEM and (b) AFM images of as-grown *b*-plane LYBO crystals with scattering centers. The horizontal edge corresponds with the (−102) cleavage plane.

In a precedent publication, it was shown that the scintillation properties of LYBO can be drastically improved after air annealing close to the T_m of LYBO.[11] Though this treatment causes a remarkable reduction in the concentration of scattering centers in LYBO, the latter do not represent the main source of non-radiative recombination, as will be seen later in the case of scattering-free crystals. In order to visualize the remaining scattering after annealing, a He-Ne laser with a five times higher power than a laser pointer was used. Figure 2 shows the images of the light path under the optical microscope before and after annealing, taken with a 100x objective under the same exposure conditions. As-grown LYBO crystals possess such a high concentration of scattering centers, even in less milky ones, that scattering spots largely overlap and a density value cannot be given. In any case, the scattering centers seem to distribute more or less homogeneously along the crystal. After annealing, the scattering path image becomes quite dark and single spots can be discerned, suggesting a reduction in the scattering center concentration of more than 1000 times. A rough estimation was carried out with the software ImageJ,[28] obtaining a value of $\sim 1 \times 10^7$ spots cm^{-2}. Despite various efforts varying annealing temperature and time, no further decrease in the concentration of scattering centers could be achieved. Therefore, we next aimed at the growth of completely scattering-free crystals.

Table I. List of stable candidates and their effective atomic numbers.

Compounds	Z_{eff}
$LiYO_2$[22]	35.6
YBO_3[23]	34.4
YB_3O_6[24]	31.2
$LiY_6O_5(BO_3)_3$[25]	35.3
$Li_2YB_5O_{10}$	28.4
$Li_3Y_2(BO_3)_3$[26]	32.4
$Li_3Y(BO_3)_2$[27]	30.9
LYBO	28.6

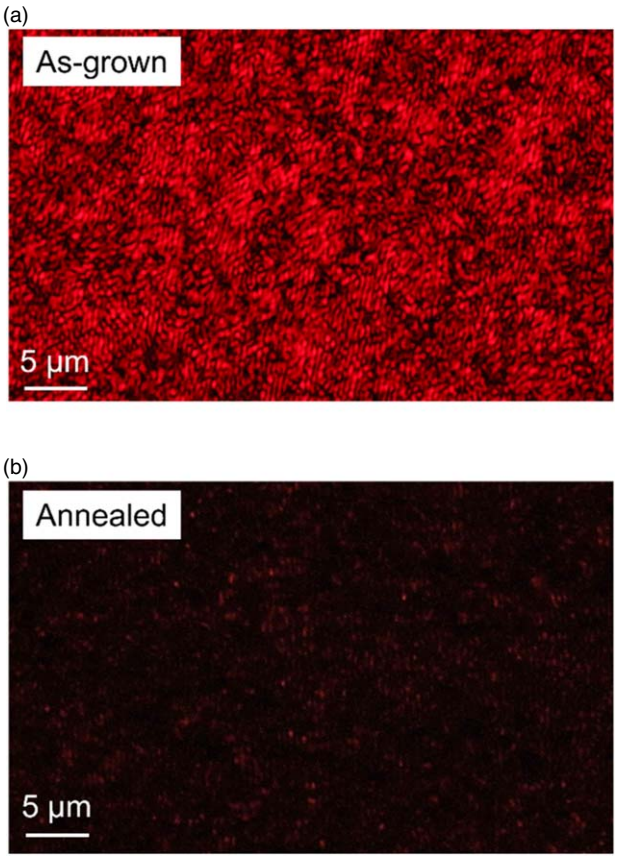

Fig. 2. Optical microscope images of the scattering path of a He-Ne laser (5 mW, 633 nm) in as-grown (a) and annealed (b) LYBO crystals.

As mentioned above, the first assumption for the formation of scattering centers was that, in the same way as $LiY_6O_5(BO_3)_3$ was gradually nucleating and growing on the crucible bottom, traces of it were dispersed in the melt and continuously segregated at the interface of the growing crystal. Under this hypothesis, it was reasonable to expect a decrease in the scattering center concentration with lower pulling speeds, since the segregation coefficient depends sensitively on the growth rate. It was found, however, that the amount of scattering centers did not depend on this parameter, which seemed to be odd. Subsequently, we focused on the cooling rate and found that the amount of scattering centers was apparently larger for a crystal that was cooled down much more slowly, which seemed to be counter-intuitive. Following this finding, instead of a gradual cooling rate, the heating of the hot zone was stopped after crystal separation, leading to a relatively quick decrease in crystal temperature. By this "quenching" method, the growth of scattering-free LYBO crystals was achieved for the first time, while demonstrating that scattering centers are not caused by the incorporation of secondary phases in the LYBO matrix during the crystal growth. The comparison between crystals with and without scattering centers, before and after annealing, in terms of light scattering of the green laser pointer and optical transmittance is given in Fig. 3. As can be expected, the scattering-free crystal exhibits the highest direct transmittance (A1), free of absorption in the whole UV-visible wavelength region, while the crystal with scattering centers presents a decreasing transmittance towards shorter wavelengths (B1). After annealing, however, both crystals

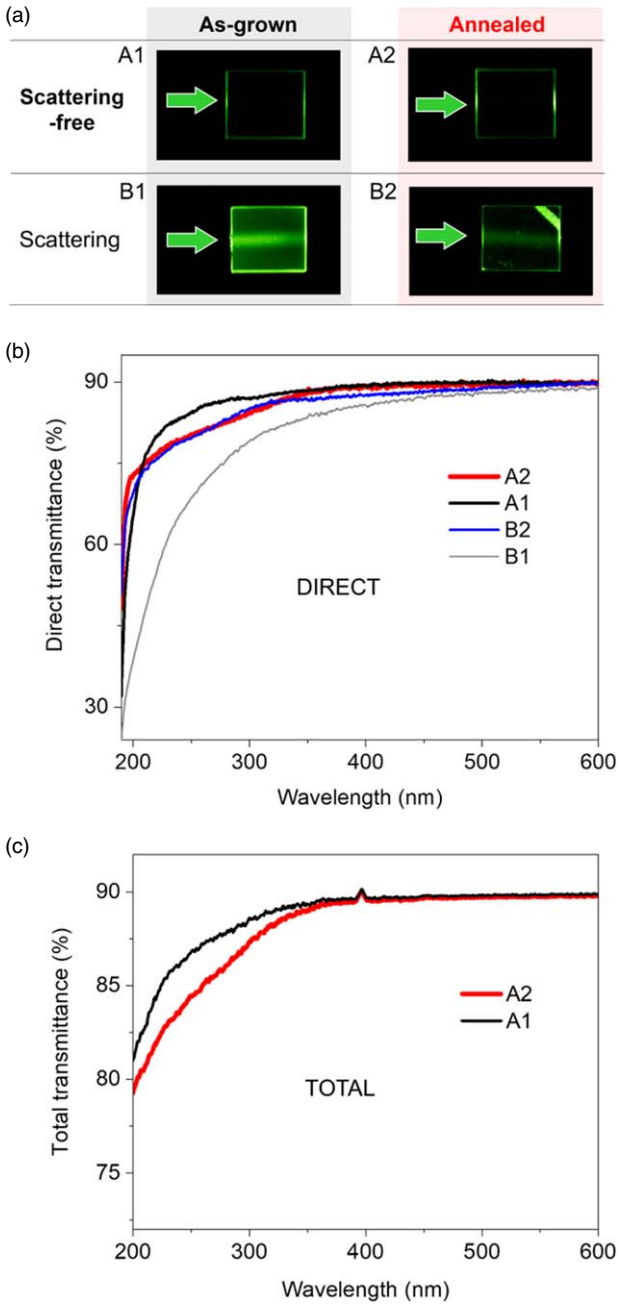

Fig. 3. (a) Scattering paths of a green laser pointer (550 nm, 1 mW) in LYBO single crystals. As-grown scattering-free crystals before (A1) and after annealing (A2); as-grown scattering crystals before (B1) and after annealing (B2). (b) Optical direct transmittance spectra of these LYBO crystals. (c) Total transmittance spectra of as-grown scattering-free LYBO crystal before and after annealing. The small peak located at 396 nm is a measurement artifact.

with (B2) and without (A2) initial scattering appear to have very similar transmission spectra, and at the same time different from as-grown crystals. In the ~200–350 nm range, the direct transmission [Fig. 3(b)] shows a slight linear drop towards short wavelengths, which could be caused by absorption and/or scattering. As shown in the case of scattering-free crystals of Fig. 3(c), total transmittance measurements with an integrating sphere indicate that the decrease in UV transparency by annealing is caused by a new absorption, whose origin needs to be investigated in more detail. Furthermore, it should be noted that below 200 nm, i.e., close to the absorption cutoff, a sharp increase in

transmittance is observed. This indicates a better crystallinity after annealing despite the newly induced UV absorbance, and as will be seen below, it's closely related to the suppression of non-radiative recombination centers.

Beyond the growth of undoped scattering-free LYBO crystals demonstrated so far, the "quenching" technique was successfully applied as well for the case of doped crystals. If previously Ce-doping was found to promote the formation of scattering centers, with the new cooling technique scattering-free Ce:LYBO single crystals could be systematically grown. In the following, the scintillation properties of the best crystal are presented.

In analogy with previous findings on scattering Ce:LYBO crystals, scattering-free ones need to be annealed under air to measure their scintillation performance.[11] The remarkable decrease in non-radiative recombination centers after annealing is attributed to a reduction in oxygen vacancies present in as-grown crystals. This hypothesis is further supported by the enhanced transmittance close to the absorption cutoff (see Fig. 3) since the valence band in LYBO crystal is defined by oxygen atoms.[29] Considering that as-grown crystals are oxygen deficient, some sort of compensating defects need to be present to keep crystal electroneutrality. Due to the large difference in cationic radii, anti-site occupations Li_Y and/or Li_B can be disregarded, and therefore only vacancies of volatile Li and B are plausible. Since boron oxide has a higher vapor pressure than lithium oxide, the predominance of V_B is more probable. This assumption is in good accordance with the ICP results given in Table II, which indicate that the Li/B ratio in LYBO crystal is higher than the theoretical value of two. In any case, by the reduction or even elimination of V_O after annealing, the defects at the atomic level (V_{Li} and V_B) have another local environment that leads to different optical features, as suggested by the slight absorption in the UV. One possibility is the formation of lithium and boron-depleted clusters with $Li_5YB_2O_7$, $Li_3YB_2O_6$, or even $Li_3Y_2(BO_3)_3$ compositions. In the particular case of as-grown scattering crystals, annealing additionally promotes the redissolution of segregated phases during the cooling process. From the two potential phases that were considered for segregation at the beginning, namely $LiYO_2$ and YBO_3, the latter is more improbable for a boron-deficient crystal. Furthermore, it is feasible that during the cooling process the local decomposition at the atomic level is favored by the presence of V_{Li} and V_B according to the breakdown reaction:

$$Li_6Y(BO_3)_3 + V_{Li} + V_B + 2V_O \rightarrow \text{“}Li_5YB_2O_7\text{”} \rightarrow LiYO_2 + Li_4B_2O_5 \quad (2)$$

whereas the first phase represents the simplest configuration of neighboring V_{Li} and V_B in LYBO, the second $LiYO_2$ is the phase visualized in FE-SEM and AFM images (Fig. 2) thanks to its relatively higher Z_{eff} and chemical stability, and the third the high-temperature stable $Li_4B_2O_5$, which would further dissociate into Li_3BO_3 and $Li_6B_4O_9$ upon cooling below ~600 °C according to the Li_2O-B_2O_3 phase diagram.[30,31]

The scintillation characteristics of a nominal 2% Ce:LYBO crystal, which has an actual Ce concentration of 0.4% relative to Y according to the ICP-OES measurement, are shown in Fig. 4 in comparison with those of the reference material for thermal neutron detection, namely the commercial Li-glass

Table II. ICP results of LYBO single crystals.

Element	Mass (mg)	Mass percentage (%)	Atomic ratio relative to Y
Li	1.969	13.2	5.91
Y	4.264	28.6	1
B	1.507	10.1	2.91

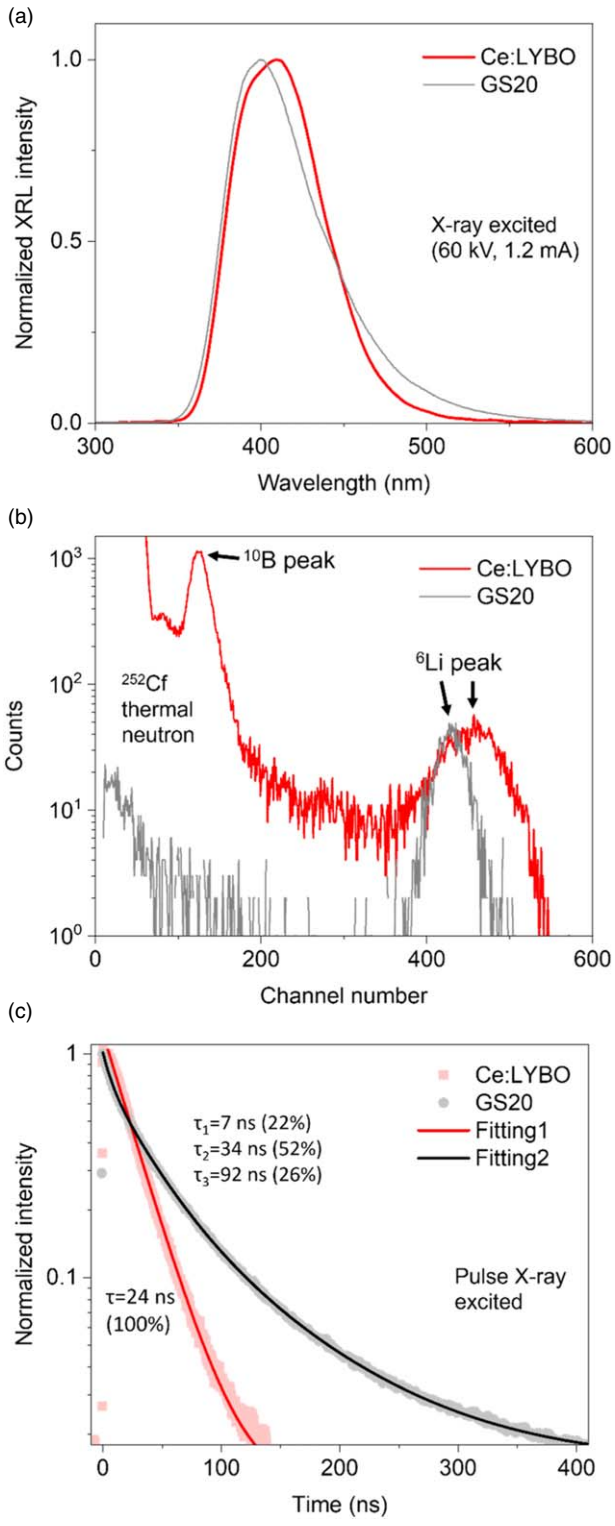

Fig. 4. Scintillation performance of nominal 2% Ce:LYBO annealed crystal in comparison with commercial Li-glass GS20. (a) Normalized XRL spectra, (b) thermal neutron pulse-height spectra, and (c) pulsed X-ray decay curves.

GS20. The XRL profile of Ce:LYBO is very similar to that of GS20,[32] thus for practical applications it matches well with standard scintillator photomultipliers, and optimum energy conversion efficiencies can be achieved. The LY as a thermal neutron scintillator was determined by PHS under ^{252}Cf irradiation. Both ^{10}B- and ^{6}Li-peaks appear at well-differentiated channels, and a value of 6200 ph/n is estimated after corresponding corrections based on PMT quantum efficiency and XRL spectra. This represents an increase of ∼800% with respect to the non-annealed value of the same crystal, thanks to the reduction in V_O, and a 36% rise in comparison with our previous record value of 4560 ph/n.[11] Therefore, the LY of Ce:LYBO is already equal to that of GS20 reference, while further improvements are expected upon optimization of other parameters such as dopant concentration. The scintillation decay upon pulsed X-ray excitation is described by a single decay with a lifetime as short as 24 ns. This value is smaller than those of most common Ce-doped scintillators[33,34] and can therefore be advantageous for time-resolved measurements.[35] On the contrary, the decay curve of GS20 is much more complex, and a three exponential fitting leads to the following lifetimes (ratios): 7 ns (22%), 34 ns (52%), and 92 ns (26%).

To conclude, scattering-free LYBO and Ce:LYBO single crystals are successfully grown for the first time. The commonly observed milky appearance in LYBO is not caused by the segregation of secondary phases during the growth, but by the decomposition of local Li- and B-deficient LYBO at the atomic level during the cooling process. This phenomenon can be prevented by thermal quenching upon cooling. The scattering centers are likely due to the participation of simple stable compounds $LiYO_2$ and $Li_4B_2O_5$, which tend to form aligned needle-like microstructures of up to 2 μm in length. As-grown crystals, with and without scattering, present oxygen vacancies that decrease transmittance and LY. These can be efficiently suppressed by annealing under air. Scattering-free Ce:LYBO crystals exhibit a higher scintillation performance, reaching for the first time a LY of 6200 ph/n, which is comparable to commercial Li-glass GS20 reference. In contrast to the complex and slow decay of the latter, Ce:LYBO exhibits a single decay with a lifetime as short as 24 ns. Current results demonstrate the potential of Ce:LYBO single crystals for thermal neutron detection applications.

Acknowledgments The authors would like to sincerely thank Mr. Satoshi Yamamoto for his kind support with crystal cutting and polishing. This work was partially supported by the Grant-in-Aid for User Facility Service in NIMS, as well as by the "Advanced Research Infrastructure for Materials and Nanotechnology in Japan (ARIM)" of the Ministry of Education, Culture, Sports, Science and Technology (JPMXP12 23NM5337).

ORCID iDs Dongsheng Yuan https://orcid.org/0000-0001-9650-2272
Daisuke Nakauchi https://orcid.org/0000-0001-6686-4694
Takumi Kato https://orcid.org/0000-0002-5650-4449
Takayuki Yanagida https://orcid.org/0000-0002-7326-5849

1) T. Yanagida, T. Kato, D. Nakauchi, and N. Kawaguchi, Jpn. J. Appl. Phys. **62**, 010508 (2023).
2) R. T. Kouzes, A. T. Lintereur, and E. R. Siciliano, Nucl. Instrum. Methods Phys. Res., Sect. A **784**, 172 (2015).
3) F. Sacchetti et al., Eur. Phys. J. Plus **130**, 53 (2015).
4) D. G. Chica, Y. He, K. M. McCall, D. Y. Chung, R. O. Pak, G. Trimarchi, Z. Liu, P. M. De Lurgio, B. W. Wessels, and M. G. Kanatzidis, Nature **577**, 346 (2020).
5) V. Popov and P. Degtiarenko, "Lithium glass scintillator neutron detector as an improved alternative to the standard 3 he proportional counter," IEEE Nuclear Science Symposuim & Medical Imaging Conference (Knoxville, TN, USA), 2011 (IEEE) p. 1819.
6) A. Syntfeld, M. Moszynski, R. Arlt, M. Balcerzyk, M. Kapusta, M. Majorov, R. Marcinkowski, P. Schotanus, M. Swoboda, and D. Wolski, IEEE Trans. Nucl. Sci. **52**, 3151 (2005).
7) T. Jin, S. Hao, Y. Shang, Z. Lei, and C. Yang, Crystals **12**, 887 (2022).
8) T. Yanagida et al., Opt. Mater. **33**, 1243 (2011).
9) F. Pino, L. Stevanato, D. Cester, G. Nebbia, L. Sajo-Bohus, and G. Viesti, J. Instrum. **10**, T08005 (2015).
10) J. P. Chaminade, O. Viraphong, F. Guillen, C. Fouassier, and B. Czirr, IEEE Trans. Nucl. Sci. **48**, 1158 (2001).
11) D. Yuan, E. G. Víllora, N. Kawaguchi, D. Nakauchi, T. Kato, T. Yanagida, and K. Shimamura, Jpn. J. Appl. Phys. **62**, 010614 (2023).
12) J. Yin, J. Zhang, J. Wang, F. Du, R. Li, S. Pan, and J. Pan, Radiat. Meas. **113**, 20 (2018).
13) A. K. Singh, M. Tyagi, S. G. Singh, B. Tiwari, D. G. Desai, S. Sen, S. S. Desai, S. S. Ghodke, and S. C. Gadkari, Nucl. Instrum. Methods Phys. Res., Sect. A **804**, 189 (2015).
14) U. Fawad, H. J. Kim, H. Park, S. Kim, and S. Khan, Nucl. Instrum. Methods Phys. Res., Sect. A **806**, 117 (2016).
15) S. Pan, J. Zhang, J. Pan, G. Ren, N. Li, Z. Wu, and Y. Heng, J. Alloys Compd. **751**, 129 (2018).
16) J. Zhang, J. Yin, Y. Jiang, F. Du, S. Pan, X. Li, and J. Pan, Radiat. Meas. **124**, 132 (2019).
17) D. Yuan, E. G. Víllora, and K. Shimamura, J. Solid State Chem. **300**, 122286 (2021).
18) T. Yanagida, Proc. Jpn. Acad. Ser. B **94**, 75 (2018).
19) T. Yanagida, G. Okada, T. Kato, D. Nakauchi, and S. Yanagida, Appl. Phys. Express **9**, 042601 (2016).
20) T. Yanagida, N. Kawaguchi, Y. Fujimoto, K. Fukuda, K. Watanabe, A. Yamazaki, and A. Uritani, J. Lumin. **144**, 212 (2013).
21) T. Yanagida, Y. Fujimoto, T. Ito, K. Uchiyama, and K. Mori, Appl. Phys. Express **7**, 062401 (2014).
22) F. Stewner and R. Hoppe, Z. Anorg. Allg. Chem. **380**, 250 (1971).
23) G. Chadeyron, M. El-Ghozzi, R. Mahiou, A. Arbus, and J. C. Cousseins, J. Solid State Chem. **128**, 261 (1997).
24) J. H. Lin, S. Zhou, L. Q. Yang, G. Q. Yao, M. Z. Su, and L. P. You, J. Solid State Chem. **134**, 158 (1997).
25) Gao and Jian-hua, Chin. J. Struct. Chem. **25**, 1175 (2006).
26) Ş. GacanoĞLu, H. GÜLer, A. Teke, and R. TÜLek, J. Boron **3**, 139 (2018).
27) S. Bräuchle and H. Huppertz, Z. Naturforsch. B **72**, 153 (2017).
28) C. A. Schneider, W. S. Rasband, and K. W. Eliceiri, Nat. Methods **9**, 671 (2012).
29) Y. Ou, W. Zhou, D. Hou, M. G. Brik, P. Dorenbos, Y. Huang, and H. Liang, RSC Adv. **9**, 7908 (2019).
30) M. M. Asadov, E. S. Kuli-zade, and S. N. Mustafaeva, AJP FIZIKA C88 (2023).
31) G. Rousse, B. Baptiste, and G. Lelong, Inorg. Chem. **53**, 6034 (2014).
32) J. Ruan, M. Xu, L. Chen, B. Sun, B. Liu, J. Liu, Z. Zhang, S. He, K. Zhao, and X. Ouyang, Nucl. Instrum. Methods Phys. Res., Sect. A **953**, 163190 (2020).
33) C. M. Combes, P. Dorenbos, C. W. E. van Eijk, K. W. Krämer, and H. U. Güdel, J. Lumin **82**, 299 (1999).
34) V. Kumar and Z. Luo, Photonics **8**, 71 (2021).
35) C. L. Wang and R. A. Riedel, Rev. Sci. Instrum. **87**, 013301 (2016).